Journal of Applied Mechanics and Technical Physics, Vol. 48, No. 6, pp. 779–788, 2007

NUMERICAL SIMULATION OF HELICAL PERTURBATIONS IN OPEN TRAPS WITH AN ELECTRON BEAM

V. P. Zhukov,[1] I. V. Shvab,[1] and A. V. Burdakov[2]

UDC 533.951

Dynamics of the plasma in open magnetic traps with an electron beam, in particular, in a GOL-3 *trap, is studied. The possibility of the formation of a resonant surface of the magnetic field and the development of helical instability caused by the presence of this surface is studied numerically.*

Key words: *plasma, tearing instability, reconnection, resonant surface.*

Introduction. Experiments in a GOL-3 multimirror trap with an electron beam (based at the Budker Institute of Nuclear Physics of the Siberian Division of the Russian Academy of Sciences) [1] are performed in the following manner. The vacuum chamber is filled by hydrogen with a concentration of $(1–3)\cdot10^{21}$ m^{-3}. Then a discharge generating the plasma is ignited, and an electron beam increasing the plasma temperature to $(1.1–2.3)\cdot10^3$ K (1.1–2.3 keV) is injected into the plasma. The maximum energy-transfer efficiency (30–40%) is observed with a density of $(1–3)\cdot10^{21}$ m^{-3}. The thus-obtained hot plasma gets cooled during $\approx$50 μsec.

Experimental data [2] show that, when the beam is interrupted, the current equal to the current in the beam flows in the center of the plasma, and the plasma current at the beam periphery flows in the opposite direction. The total current intensity is rather low. This current configuration becomes destroyed during a time substantially smaller than the time of ohmic decay. The rapid disintegration of the current configuration is assumed to be caused by the evolution of tearing instability. This phenomenon is studied in the present paper.

Tearing instability, which plays an important role in plasma dynamics in tokamaks, is the reason for relaxation (saw-tooth) oscillations inherent in all tokamaks. Owing to the evolution of this instability [3, 4], the intensity of the current flowing over the plasma rapidly decreases, and the thermal energy of the plasma is transferred from the center to the periphery. For tokamaks, these phenomena have been well studied. In particular, there are many papers with numerical simulations of tearing instability, where two-dimensional [4–10] and three-dimensional [11, 12] models were used in approximations of reduced [5–8] and nonreduced [9–12] one-fluid [4, 11, 12] and two-fluid [5–8, 10] magnetohydrodynamics.

Modeling of tearing instability in an open trap with an electron beam, which is described in the present paper, was a pioneering study. The challenge was to investigate the possibility of the formation of a magnetic configuration with a resonant surface of the magnetic field and the development of tearing instability in such a configuration and to quantify characteristics of the flow caused by the development of this instability. In particular, it was necessary to estimate the time of failure of the current configuration.

We used one- and two-dimensional one-fluid magnetohydrodynamic (MHD) models numerically implemented with the use of finite-difference algorithms. The electron beam was taken into account by additional terms in equations for the magnetic field. Corrugation and the presence of end faces were neglected in this model. Conductivity of the plasma outside the beam was assumed to be equal to the Coulomb conductivity at a temperature of $1.16\cdot10^6$ K (100 eV). Because of the beam instability, the flow is turbulent, and the plasma resistance in the region occupied by the beam is greater than the Coulomb value. The exact value of anomalous resistance is unknown;

[1]Institute of Computational Technologies, Siberian Division, Russian Academy of Sciences, Novosibirsk 630090; shva@ict.nsc.ru. [2]Budker Institute of Nuclear Physics, Siberian Division, Russian Academy of Sciences, Novosibirsk 630090. Translated from Prikladnaya Mekhanika i Tekhnicheskaya Fizika, Vol. 48, No. 6, pp. 3–14, November–December, 2007. Original article submitted April 26, 2006; revision submitted December 6, 2006.

therefore, the plasma resistance inside the beam was varied in calculations from 10 to 100 Coulomb values. When the beam is interrupted, its anomalous resistance vanishes. The resistance of the hot plasma is substantially lower than the resistance of the plasma at a temperature of $1.16 \cdot 10^6$ K (100 eV). The development of tearing instability is determined by the local value of resistance on the resonant surface. This surface is outside the beam region; correspondingly, the temperature on the resonant surface is significantly lower than $1.16 \cdot 10^7$ K (1 keV). Investigation of the temperature distribution due to plasma heating by the beam is an independent difficult problem. In the present work, for simplicity, the plasma resistance after beam interruption was assumed to be constant and equal to the Spitzer resistance at a temperature of $1.16 \cdot 10^6$ K (100 eV).

Tearing instability has been well studied in the case without the beam and without strong gradients of conductivity. It should be noted that strong gradients of conductivity usually occur at the edge of the beam near the resonant surface. Such a situation has not been considered previously. For instance, the conductivity in tokamaks changes at distances of the order of a small radius of the plasma and does not produce any significant effect on tearing instability.

1. Mathematical Formulation of the Problem. Let us consider the mathematical formulation of the problem. The original MHD equations of a one-fluid two-temperature plasma have the following form [13, 14]:

$$\rho \frac{\partial \boldsymbol{V}}{\partial t} = -\nabla p + \frac{1}{c}(\boldsymbol{j} \times \boldsymbol{H}) + \nu \Delta \boldsymbol{V} + \frac{\nu}{3} \nabla \operatorname{div} \boldsymbol{V},$$

$$\frac{1}{\gamma_e - 1}\Big(\frac{\partial p_e}{\partial t} + \operatorname{div}(\boldsymbol{V} p_e)\Big) = -p_e \operatorname{div} \boldsymbol{V} + \operatorname{div}\Big(\chi_e \nabla T_e + \chi_{\|e} \boldsymbol{h}(\boldsymbol{h} \nabla T_e)\Big) + \frac{(\boldsymbol{j} - \boldsymbol{j}_0)^2}{\sigma},$$

$$\frac{1}{\gamma_i - 1}\Big(\frac{\partial p_i}{\partial t} + \operatorname{div}(\boldsymbol{V} p_i)\Big) = -p_i \operatorname{div} \boldsymbol{V} + \operatorname{div}\Big(\chi_i \nabla T_i + \chi_{\|i} \boldsymbol{h}(\boldsymbol{h} \nabla T_i)\Big) + Q_\nu, \tag{1}$$

$$\frac{\partial \boldsymbol{H}}{\partial t} = \operatorname{rot}\Big([\boldsymbol{V}\boldsymbol{H}] - \frac{c}{\sigma}(\boldsymbol{j} - \boldsymbol{j}_0)\Big), \qquad \frac{\partial \rho}{\partial t} + \operatorname{div} \rho \boldsymbol{V} = 0,$$

$$\operatorname{div} \boldsymbol{H} = 0, \qquad \boldsymbol{j} = \frac{c}{4\pi} \operatorname{rot} \boldsymbol{H}, \qquad T_{i,e} = \frac{p_{i,e}}{\rho}, \qquad \boldsymbol{h} = \frac{\boldsymbol{H}}{|\boldsymbol{H}|}.$$

Here ρ, $\boldsymbol{V}$, and σ are the plasma density, velocity, and conductivity, respectively, $\boldsymbol{j}_0$ is the density of the current intensity in the beam, $\boldsymbol{H}$ is the magnetic field, ν is the viscosity, Q_ν is the plasma heating due to the work of viscous forces [14], $p_{i,e}$ and $T_{i,e}$ are the plasma pressure and temperature, respectively, $\chi_{\|e,i}$ and $\chi_{e,i}$ are the coefficients of longitudinal and isotropic thermal conductivity, respectively, and $\gamma_e = \gamma_i = \gamma = 5/3$ are the ratios of specific heats of electrons and ions; the subscripts i and e refer to ions and electrons, respectively.

Let us consider an MHD flow possessing helical symmetry. In this case, the scalar quantities and the cylindrical components of the vectors (r, φ, and z) depend on coordinates in such a manner that the following relation holds:

$$\frac{\partial}{\partial z} = -\frac{1}{R}\frac{\partial}{\partial \varphi}. \tag{2}$$

Under helical symmetry, various functions depend on the value of $\varphi - z/R$ rather than on φ and z separately. Below, we understand φ as $\varphi - z/R$. For the GOL-3 facility, the parameter is $R = z_0/(2\pi a N)$. Here $z_0 = 1200$ is the facility length in centimeters, $a = 5$ is the facility radius in centimeters, and N is the mode number (integer).

There are reasons to believe that the mode dominating under GOL-3 conditions is the mode with $N = 1$ (see below); therefore, we used $N = 1$ in what follows. The calculations show that the results are little different in the presence of other modes (e.g., the mode with $N = 0$).

In the case of helical symmetry (2), it is reasonable to use the g and s components of the vectors, which are related to the φ and z components as follows:

$$f_s = f_\varphi - (r/R) f_z, \qquad f_g = f_z + (r/R) f_\varphi.$$

It is also convenient to introduce vector components (for brevity, we call them the Cartesian coordinates of the vector) related to the r and φ components by

$$f_x = f_r \cos\varphi - f_\varphi \sin\varphi, \qquad f_y = f_r \sin\varphi + f_\varphi \cos\varphi.$$

As φ is understood as $\varphi - z/R$, these components coincide with real Cartesian coordinates only as $R \to \infty$.

As the length of the GOL-3 facility is limited, symmetry (2) is invalid. Let us elucidate when the edge effects can be neglected. This question is rather complicated. To estimate the influence of the edge effects, we assume the magnetic field to be "frozen" into the end faces of the chamber. Because of this assumption, the longitudinal field entrained by the transversely moving plasma is deformed. As a result, a transverse field is generated. In this case, as is demonstrated below, plasma displacement is of the order of the neutral surface radius and is approximately equal to $a/2$. Correspondingly, the magnitude of the transverse field generated owing to the presence of the end faces is of the order $H_z a/(2z_0) \approx 0.1$ kGs. For this field to exert no strong influence on the flow, the field should be substantially less intense than the transverse magnetic field generated by the longitudinal current flowing over the plasma. The value of the transverse magnetic field is of the order of 1 kGs. Thus, the approximation used is validated. In reality, the restriction on the ratio a/z_0 is far from being so rigorous because of the GOL-3 structure.

Magnetic field corrugation is neglected. As plasma cooling due to heat outflow to the end faces of the facility occurs during ≈ 50 μsec and the duration of the processes considered is less than 10 μsec, the heat flux toward the end faces of the facility can also be neglected.

Further we use dimensionless quantities. The facility radius is used as a length scale. The calculations were performed with the following characteristic values: strength of the longitudinal magnetic field $H_z = 50$ kGs, density $\rho_* = 10^{21}$ m^{-3}, velocity (Alfvén velocity calculated on the basis of the toroidal magnetic field) $V_\mathrm{A} = H_z/\sqrt{4\pi\rho_*} = 3.48 \cdot 10^6$ m/sec, time $a/V_\mathrm{A} = 1.44 \cdot 10^{-8}$ sec, pressure $H_z^2/(4\pi)$, etc.

With allowance for these facts, Eqs. (1) acquire the form

$$\rho\Big(\frac{\partial V_x}{\partial t} + (\boldsymbol{V}\nabla)V_x - \frac{V_z V_y}{R}\Big) = \nu\Big(\Delta V_x - \Big(V_x - 2\,\frac{\partial V_y}{\partial\varphi}\Big)R^{-2}\Big) + F_x,$$

$$\rho\Big(\frac{\partial V_y}{\partial t} + (\boldsymbol{V}\nabla)V_y - \frac{V_z V_x}{R}\Big) = \nu\Big(\Delta V_y - \Big(V_y + 2\,\frac{\partial V_x}{\partial\varphi}\Big)R^{-2}\Big) + F_y, \tag{3}$$

$$\rho\Big(\frac{\partial V_z}{\partial t} + (\boldsymbol{V}\nabla)V_z\Big) = \nu\Delta V_z + F_z;$$

$$(F_r, F_s) = -\nabla(p - (\nu/3)\,\mathrm{div}\,\boldsymbol{V}) + G^{-1}(-\nabla(H_g^2/2) + j_g\nabla\psi),$$

$$F_g = (\boldsymbol{H}\nabla)H_g, \qquad p = p_i + p_e, \qquad j_g = -\Delta_g(\psi) + 2H_g/(RG); \tag{4}$$

$$\frac{\partial\psi}{\partial t} + \boldsymbol{V}\nabla\psi = -\eta(j_g - j_0); \tag{5}$$

$$\frac{\partial H_g}{\partial t} = G\,\mathrm{div}\,(G^{-1}\boldsymbol{S}) + \frac{2}{RG}\,\frac{\partial\psi}{\partial t}; \tag{6}$$

$$\boldsymbol{S} = -\boldsymbol{V}H_g + V_g\boldsymbol{H} + \eta\nabla H_g; \tag{7}$$

$$\frac{\partial\rho}{\partial t} + \mathrm{div}\,(\boldsymbol{V}\rho) = 0,$$

$$\frac{1}{\gamma_i - 1}\Big(\frac{\partial p_i}{\partial t} + \mathrm{div}(\boldsymbol{V}p_i)\Big) = -p_i\,\mathrm{div}\,\boldsymbol{V} + \mathrm{div}\,(\chi_{\|i}\boldsymbol{h}(\boldsymbol{h}\nabla)T_i) + \mathrm{div}\,(\chi_i\nabla T_i) + Q_\nu,$$

$$\frac{1}{\gamma_e - 1}\Big(\frac{\partial p_e}{\partial t} + \mathrm{div}(\boldsymbol{V}p_e)\Big) = -p_e\,\mathrm{div}\,\boldsymbol{V} + \mathrm{div}\,(\chi_{\|e}\boldsymbol{h}(\boldsymbol{h}\nabla)T_e) + \mathrm{div}\,(\chi_e\nabla T_e) + Q_\eta, \tag{8}$$

$$Q_\eta = \eta(j_r^2 + G^{-1}(j_s^2 + (j_g - j_0)^2)), \qquad (j_r, j_s) = \Big(\frac{1}{r}\,\frac{\partial H_g}{\partial\varphi}, -\frac{\partial H_g}{\partial r}\Big);$$

$$\boldsymbol{H} = (H_r, H_s) \equiv \Big(\frac{1}{r}\,\frac{\partial\psi}{\partial\varphi}, -\frac{\partial\psi}{\partial r}\Big), \qquad \boldsymbol{h} = \frac{\boldsymbol{H}}{(H_r^2 + G^{-1}(H_s^2 + H_g^2))^{1/2}}, \tag{9}$$

$$T_{i,e} = p_{i,e}/\rho, \qquad G = 1 + r^2/R^2.$$

Here ψ is the poloidal magnetic flux (g component of the potential vector), H_g is the g component of the magnetic field, η is the plasma resistance, Q_η is the ohmic heating, $\chi_{\|i,e}$ and $\chi_{i,e}$ are the dimensionless coefficients of longitudinal and isotropic thermal conductivity, respectively, and $\boldsymbol{e}$ is a vector with components $e_r = e_s = 0$ and $e_g = 1$. The differential operators used in Eqs. (3)–(9) have the following form [9, 15]:

$$\operatorname{div}(\boldsymbol{f}) = \frac{1}{r}\frac{\partial(rf_r)}{\partial r} + \frac{1}{r}\frac{\partial f_s}{\partial \varphi}, \quad (\nabla a)_r = \frac{\partial a}{\partial r}, \quad (\nabla a)_s = \frac{1}{r}\frac{\partial a}{\partial \varphi}, \quad (\boldsymbol{f}\nabla)a = f_r\frac{\partial a}{\partial r} + f_s\frac{1}{r}\frac{\partial a}{\partial \varphi}.$$

The equations for velocity (3) written in Cartesian coordinates have a simpler form. In addition, the use of Cartesian coordinates is of principal importance for constructing the finite-difference algorithm [16] used to solve the problem posed.

The initial conditions are chosen to be an axisymmetric configuration with a neutral surface and a small perturbation of the magnetic flux violating this symmetry:

$$\psi = \psi_0(r) + \psi_p r(1 - r^2)\cos\varphi.$$

Here $\psi_p = 10^{-4}$ is the perturbation amplitude; the function ψ_0 corresponds to the current strength distribution:

$$j_g(0) = \begin{cases} -5 \text{ kA}/(\pi r_1^2), & r < r_1 = 4 \text{ cm}, \\ 0, & r > r_1. \end{cases}$$

It was assumed thereby that $H_z = 1$. The plasma density was constant ($\rho = 1$), and the plasma velocity was $\boldsymbol{V} = 0$. The plasma pressures p_e and p_i were either chosen from the condition of plasma equilibrium in the magnetic field or prescribed in the form

$$p_e = p_i = \begin{cases} p_0, & r < r_0 = 2.5 \text{ cm}, \\ p_0/10, & r > r_0. \end{cases}$$

The dimensionless quantity p_0 was set to be $1.584 \cdot 10^{-3}$, which corresponds to a temperature $T_e = T_i = 1.16 \times 10^6$ K (100 eV).

Thus, the initial configuration is not an equilibrium one. Because of the large strength of the longitudinal field, a small displacement of the plasma establishes the necessary equilibrium. Moreover, heating caused by the beam leads to fast and intense heating of the plasma. Therefore, a particular form of the initial pressure distribution is not principally important for the processes under study. It should be noted that experimental data on the radial distribution of pressure are unavailable.

The beam density j_0 was set in the form

$$j_0 = \begin{cases} 30 \text{ kA}/(\pi r_0^2), & r < r_0 = 2.5 \text{ cm}, \quad t < 8.64 \ \mu\text{sec}, \\ 0, & r > r_0 = 2.5 \text{ cm} \quad \text{or} \quad t < 8.64 \ \mu\text{sec}. \end{cases}$$

The plasma resistance was calculated by the formulas

$$\eta = \begin{cases} \eta_b \gg \eta_0, & r < r_0 = 2.5 \text{ cm}, \quad t < 8.64 \ \mu\text{sec}, \\ \eta_b + (\eta_0 - \eta_b)(r - r_0)/\delta, & r_0 < r < r_0 + \delta, \quad t < 8.64 \ \mu\text{sec}, \\ \eta_0, & r > r_0 + \delta \quad \text{or} \quad t > 8.64 \ \mu\text{sec}. \end{cases}$$

In calculations, the width of the transitional zone δ was assumed to be 0.5 cm. Such a distribution of η indicates that the presence of the beam leads to the development of small-scale beam instability, which is the reason for the emergence of anomalous resistance [2].

The problem was solved in the domain $0 \leqslant r \leqslant 1$, $0 \leqslant \varphi \leqslant 2\pi$. At the boundary $r = 1$, we assumed that

$$\boldsymbol{V} = 0, \qquad T_{i,e} = \text{const} \tag{10}$$

and set the tangential components of the electric field ($E_g = E_s = 0$), which are the conducting wall conditions:

$$\psi = \text{const}, \qquad \frac{\partial H_g}{\partial r} = 0. \tag{11}$$

The plasma viscosity is usually low. In dimensionless calculations, we have the coefficient $\nu \leqslant 0.1\eta$, and its value has no effect on the calculation results.

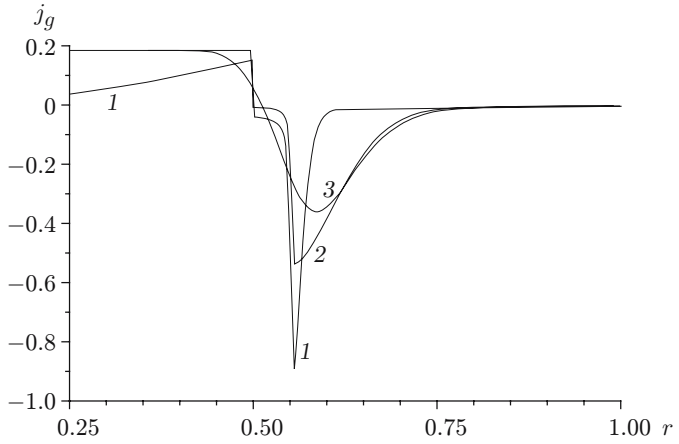

Fig. 1. Current density j_g versus the radius r for $t = 50$ (1), 600 (2), and 700 (3).

2. Finite-Difference Scheme. The problem of tearing instability is one of many hydrodynamic problems with a natural cylindrical coordinate system (r, φ, z). In this case, the boundary of the computational domain and the current layer (region of high gradients) are located on circumferences. The origin is not physically defined. It is known that solving such problems numerically involves difficulties in obtaining a smooth solution in the vicinity of the origin, because the grid step in the azimuthal direction decreases as $r \to 0$. In the vicinity of $r = 0$, there arises nonphysical small-scale instability leading in some cases to the solution decay.

Zhukov [16] provided a detailed description of a finite-difference scheme that allows one to avoid the difficulties mentioned above. The scheme [16] is designed for solving the problem of the development of tearing instability in tokamaks in the approximation of the two-fluid MHD model.

The scheme proposed in [16] is a scheme that involves splitting with respect to spatial variables and possesses the property of full approximation [17] and a sufficient reserve of stability. The scheme [16] is implemented through an iterative process rapidly converging to an absolutely implicit scheme. The optical time step in this scheme is actually restricted by the Courant number in the radial direction. This restriction has a physical nature and is fairly acceptable.

To solve problem (3)–(11), Zhukov [16] introduced a grid refined in the neutral layer in the r direction with a step r_i $(i = 0, \ldots, i_0 + 1)$. For this grid, $r|_{i=0} = 0$ and $(r_{i_0} + r_{i_0+1})/2 = 1$. With respect to φ, a uniform grid with a step $h_\varphi = 2\pi/j_0$ is used: $\varphi_j = jh_\varphi$ $(j = 1, \ldots, j_0)$. With respect to j, periodicity with a period j_0 is assumed, where j_0 is an integer. At points r_i and φ_j, which are called integer points, the values of the parameters p, p_e, T, ρ, H_g, χ, and η are calculated. Semi-integer points $r_{i+1/2} = (r_{i+1} + r_i)/2$ $(i = 0, \ldots, i_0)$ and $\varphi_{j+1/2} = h_\varphi(j + 1/2)$ are also introduced, where the values of A_g, j_g, $\boldsymbol{V}$, and ν are calculated.

In the present work, the scheme [16] was modified to solve the problem posed above.

3. Calculation Results. Results of one-dimensional and two-dimensional numerical simulations of helical perturbations in open traps with an electron beam are presented below.

3.1. *One-Dimensional Case.* The solution was assumed to be independent of φ $(\psi_p = 0)$. The calculations were performed with a resistance outside the beam $\eta_0 = 4.5 \cdot 10^{-6}$ corresponding to the Coulomb value at a temperature of $1.16 \cdot 10^6$ K (100 eV). The presence of beam instability leads to a significant increase in the plasma resistance in the region occupied by the beam, as compared with the Coulomb value. The evolution of the plasma flow was considered for $\eta_b = 100\eta_0$.

Figure 1 shows the current density as a function of the radius at the beginning of the process $(t = 50)$, before beam interruption $(t = 600)$, and at a certain time after beam interruption $(t = 700)$. The calculation results show that the current density at the center tends to the current density in the beam, because of nonuniform resistance of the plasma and the presence of the beam, while a current with the opposite sign emerges at the periphery. The magnetic field H_s and magnetic flux ψ [see Eqs. (5) and (9)] corresponding to this current at different times are shown in Fig. 2. It follows from Fig. 2 that a resonant surface of the magnetic field is formed by the end of the beam action, i.e., H_s changes its sign at $r = 0.6$. Hence, tearing instability may develop. It is seen in Fig. 2b that

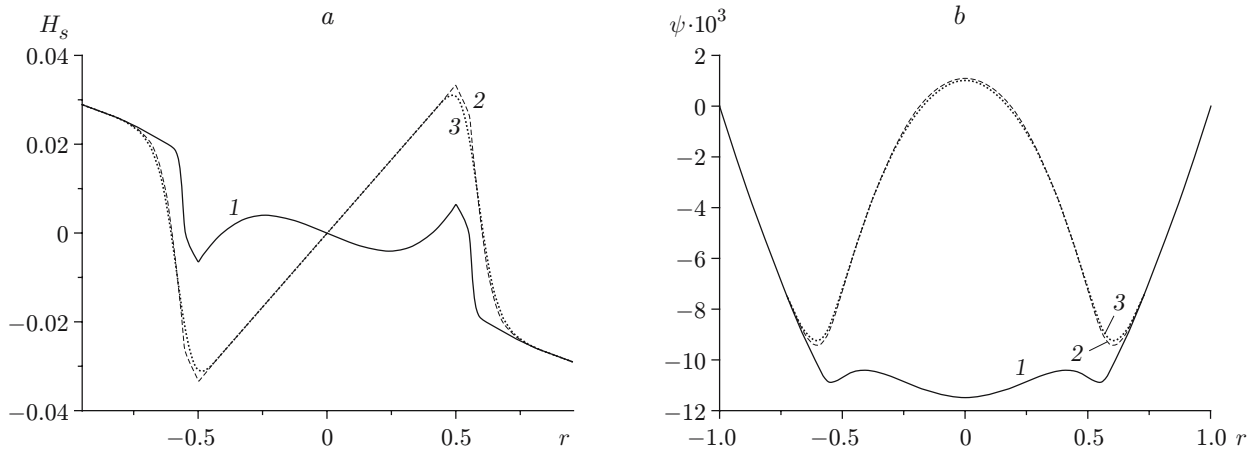

Fig. 2. Magnetic field (a) and magnetic flux (b) for $t = 50$ (1), 600 (2), and 700 (3).

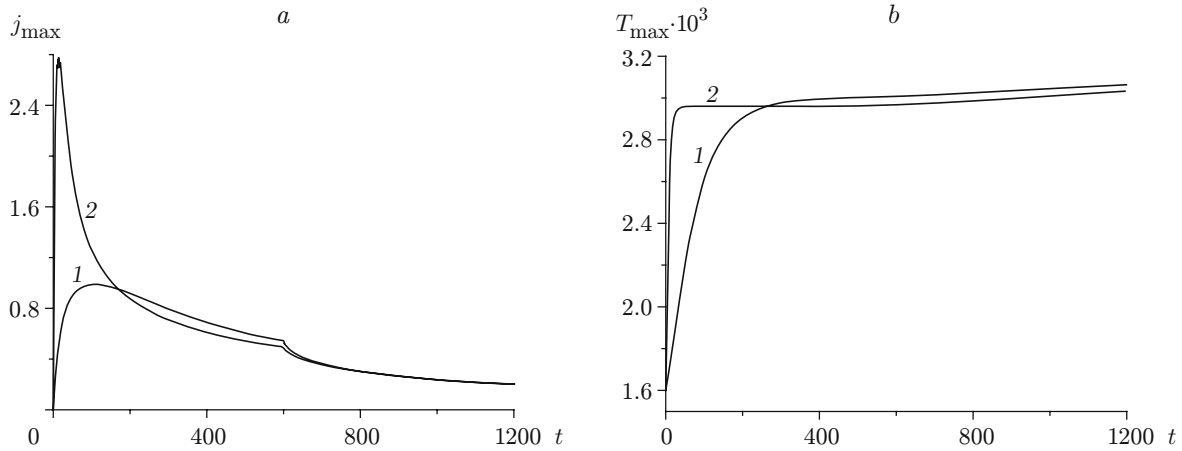

Fig. 3. Time evolution of the maximum absolute values of the current density (a) and plasma temperature (b): curves 1 and 2 refer to $\eta_b = 100\eta_0$ and $1000\eta_0$, respectively.

the magnetic flux at the center is greater than that at the boundary $r = 1$. Therefore, tearing instability may lead to elimination of the external flow and plasma ejection onto the wall.

Figure 3a shows the maximum absolute value of the current density versus time for $\eta_b = 100\eta_0$ and $1000\eta_0$. Note that the maximum absolute value of j_z is reached at a point corresponding to a negative current. The current density is seen to increase faster for the higher value of η_b at the initial time. The reason is a more nonuniform resistance at $\eta_b = 1000\eta_0$ than at $\eta_b = 100\eta_0$. It is also worth noting that the drastic increase in $j_{\max}$ is caused by the formation of the current with the opposite sign. A significant decrease in the current density immediately after beam interruption is caused by disappearance of beam instability and by the plasma resistance becoming uniform. In this case, the effect of current collection [4] after beam interruption vanishes, and the current density distribution becomes more smooth (curve 3 in Fig. 1). At the moment of beam interruption, the maximum absolute value of the current density depends only weakly on η_b.

Note that the change in the current density is mainly determined by the functions η_b and j_0. The calculations show that the results of solving Eqs. (5) and (6) with $V = 0$ almost coincide with those described above.

Figure 3b shows the maximum plasma temperature $T_{\max} = T_e + T_i$ versus time for different values of η_b. The temperature is seen to increase faster for the higher initial value of η_b. At high values of t, however, the value of $T_{\max}$ is only weakly dependent on η_b.

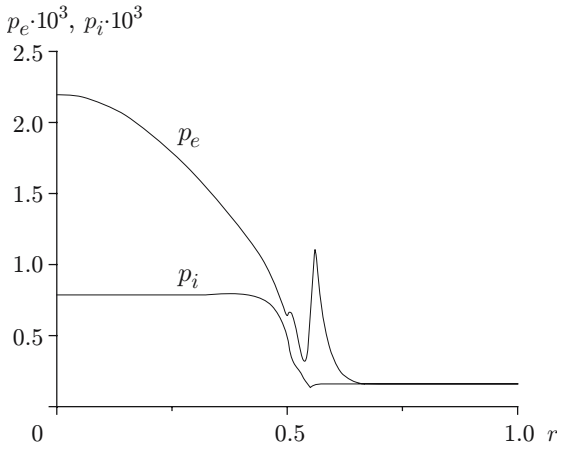

Fig. 4. Radial distributions of ion and electron pressures at the moment of beam interruption.

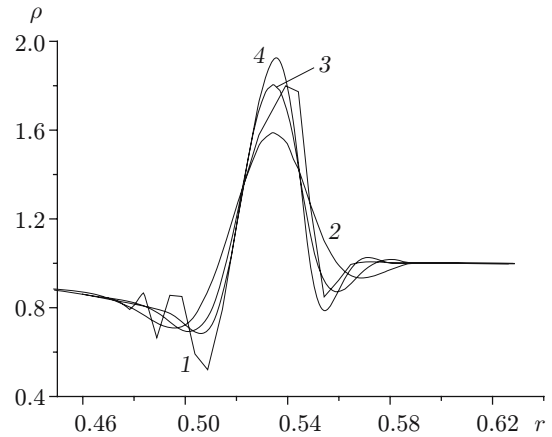

Fig. 5. Radial distributions of the plasma density for different numbers of grid nodes I_0 and different values of the parameter ε at the time $t = 600$: 1) $\varepsilon = 0$ and $I_0 = 200$; 2) $\varepsilon = 10^{-11}$ and $I_0 = 200$; 3) $\varepsilon = 0.25 \cdot 10^{-11}$ and $I_0 = 400$; 4) $\varepsilon = (1/16) \cdot 10^{-11}$ and $I_0 = 800$.

Figure 4 shows the radial distributions of ion and electron pressures at the moment of beam interruption. It is seen that the electron pressure is higher than the ion pressure, which is caused by ohmic heating.

The configuration emerging owing to the presence of the beam and a high gradient of plasma conductivity is unstable for several modes (in particular, for $N = 1$ and 0). Our choice of the mode with $N = 1$ is based on the assumption that this is a fundamental mode, because the reserve of the magnetic fluxes of both signs reaches the greatest value for the mode with $N = 1$. In addition, results of preliminary three-dimensional calculations are available, which confirm that the mode with $N = 1$ is dominating. We also performed calculations for the mode with $N = 0$ (the second one in terms of the magnitude of magnetic fluxes of different signs), which turned out to be qualitatively consistent with results for the mode with $N = 1$ described in the present work (in particular, the order of magnitude of the time of instability development was the same).

As the scheme used in calculations has the second order of approximation with respect of the spatial variable, numerical dispersion, which exerts the greatest effect on the distribution of the plasma density in the region of the highest gradients (at the beam periphery), leads to the formation of small-scale perturbations (Fig. 5). To suppress the dispersion, we replaced Eq. (7) by the equation

$$\frac{\partial \rho}{\partial t} + \operatorname{div}(\boldsymbol{V}\rho) = -\varepsilon \Delta^2 \rho.$$

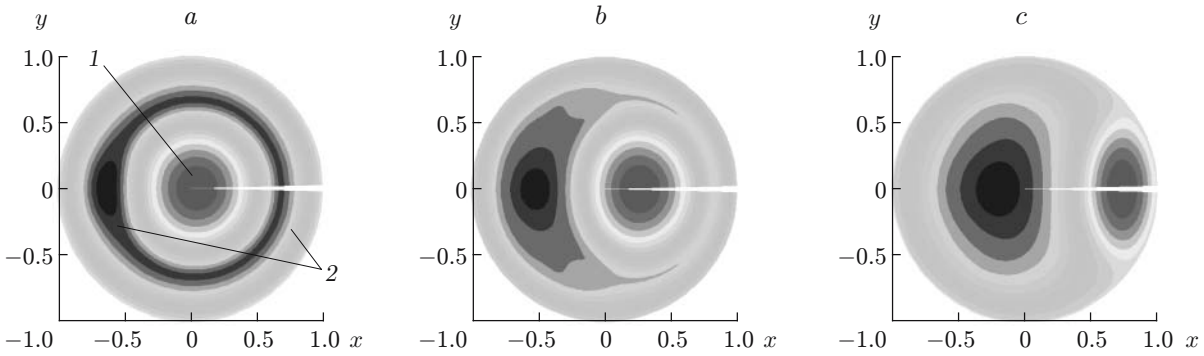

Fig. 6. Magnetic field isolines for $t = 500$ (a), 800 (b), and 1800 (c); regions indicated by 1 and 2 contain a positive and a negative magnetic flux, respectively.

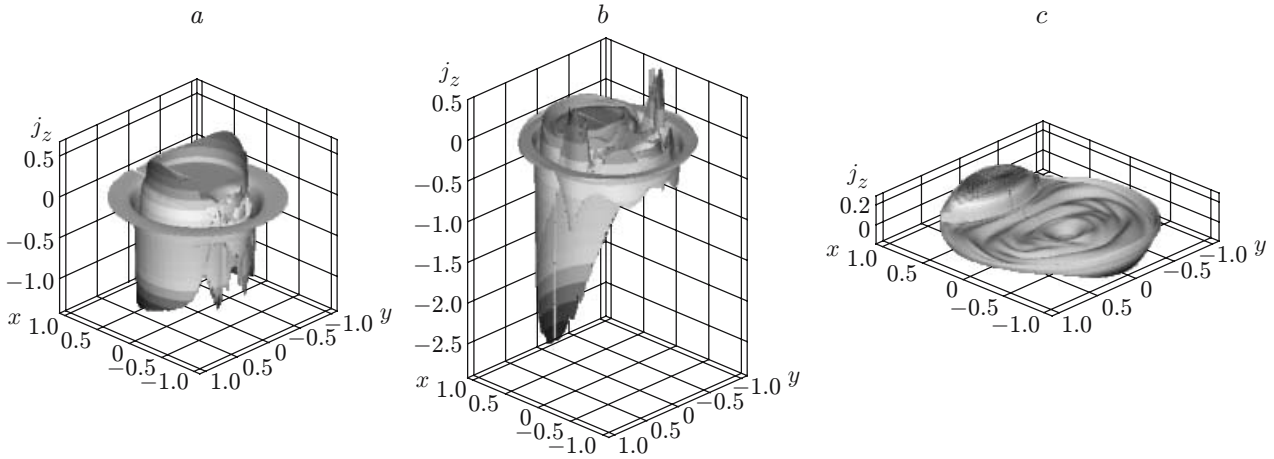

Fig. 7. Distributions of the current density along the x and y coordinates for $t = 500$ (a), 800 (b), and 1800 (c).

The term $\varepsilon\Delta^2\rho$ substantially suppresses small-scale perturbations and weakly affects long-wave disturbances. Figure 5 shows the radial distributions of the plasma density for different numbers of grid nodes I_0 and different values of the parameter ε (it was assumed that $\varepsilon \sim I_0^{-2}$). It follows from Fig. 5 that the distribution is smooth for $\varepsilon \neq 0$, and convergence is observed with increasing I_0. With I_0 being varied, the plots of the remaining functions change insignificantly. Note that tearing instability is mainly determined by the distribution of the electric current and the magnetic field induced by the latter, while the distribution of the plasma density produces only a weak effect on the development of tearing instability [10].

3.2. *Two-Dimensional Case.* In the two-dimensional case, a small perturbation of the magnetic flux ψ_p leads to the emergence of tearing instability. Figure 6 shows the isolines of the magnetic field. The figure shows the beginning of the reconnection process ($t = 500$), developed instability ($t = 800$), and the moment when the internal flow reaches the boundary and a quasi-steady configuration is established ($t = 1800$). In the case considered, the internal magnetic flux is not completely eliminated in the course of reconnection, and the quasi-steady configuration is not axially symmetric.

Figure 7 shows the x and y distributions of the current density. Instability (loss of axial symmetry) is seen to appear already at the stage of the beam action ($t = 500$). After beam interruption ($t = 800$), the current layer becomes clearly expressed, which characterizes strong instability. At the end of reconnection ($t = 1800$), the current density is low.

Figure 8 shows the distributions of the ion pressure at different times. Because of the instability development, the high-pressure region moves toward the cold boundary. Hence, these is a strong heat flux toward the boundary.

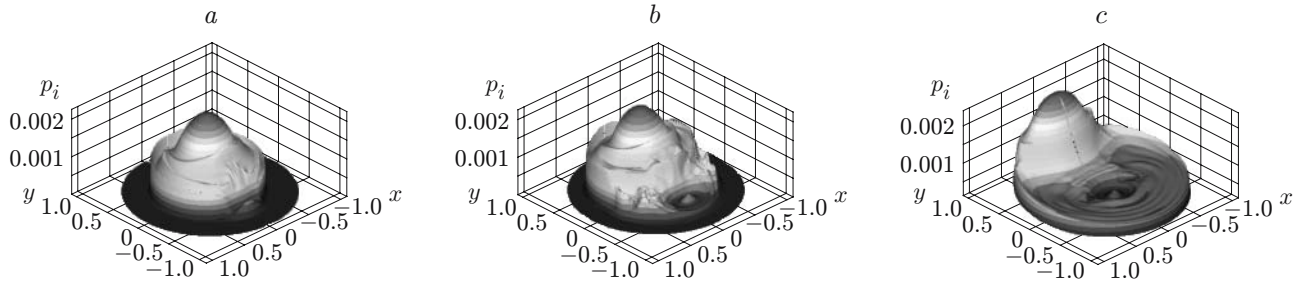

Fig. 8. Distributions of the ion pressure along the x and y coordinates for $t = 500$ (a), 800 (b), and 1800 (c).

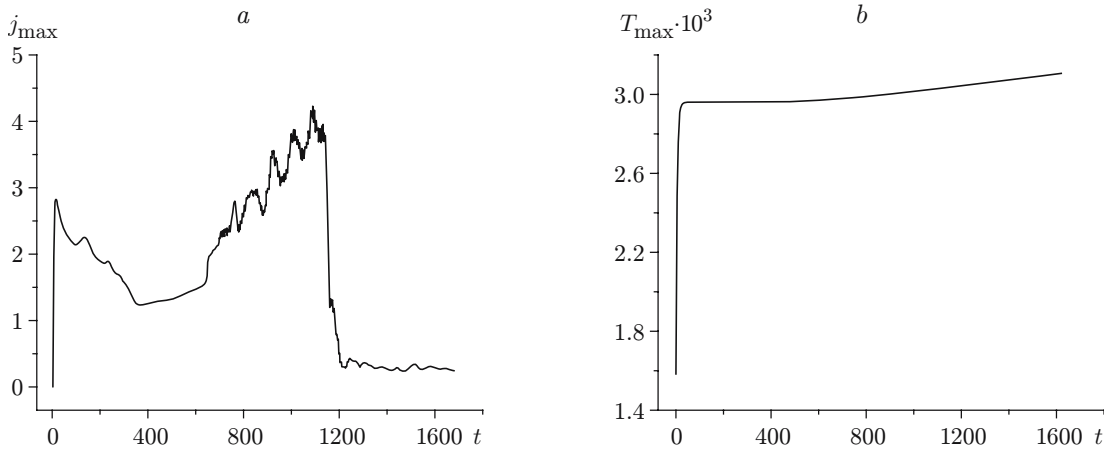

Fig. 9. Maximum absolute values of the current density (a) and plasma temperature (b) versus time.

Figure 9a shows the time evolution of the maximum absolute value of the current density. A drastic increase in the current density at the initial time is caused by the formation of a current with the opposite sign. Then the current density decreases because of the plasma resistance. The effect of tearing instability on the dependence $j_{\max}(t)$ during the beam action is small. After beam interruption, the maximum of the current density nonuniformly increases, which is caused by the rapid development of tearing instability. When the negative magnetic flux surrounding the positive magnetic flux vanishes, instability disappears, which results in a drastic decrease in the current density.

Figure 9b shows the time evolution of the maximum plasma temperature. Note that the maximum value of temperature drastically increases at the initial time and then remains almost unchanged, in contrast to the total thermal energy.

Conclusions. Thus, the following results were obtained within the framework of the one-dimensional model.

The evolution of the current density distribution is mainly determined by the magnitude of resistance and the beam current strength. Plasma motion has almost no effect on the current density.

The greater the ratio of the plasma resistances inside and outside the beam, the greater the maximum density of the reverse current. The maximum reverse current density in space and time depends substantially on the ratio of resistances. At the moment of beam interruption, however, the current density distribution depends weakly on the anomalous resistance.

The greater the ratio of the plasma resistances inside and outside the beam, the faster the increase in plasma temperature due to ohmic heating, but the plasma temperature at the moment of beam interruption is independent of this ratio.

The calculations predict that the plasma temperature increases approximately to $3.5 \cdot 10^6$ K (300 eV). Its value in experiments reaches $1.16 \cdot 10^7$ K (1 keV). Hence, the energy transfer directly from the beam to the plasma has to be taken into account. The calculations also ignored the heat flux onto the end faces of the chamber. Possibly, allowance for these factors in the numerical model and comparisons of the results obtained with experimental data

will allow one to quantify these processes. It should be noted that the distribution of the most important quantity (magnetic field) depends only weakly on pressure and temperature.

The results obtained within the framework of the two-dimensional model allow the following conclusions to be drawn.

Instability starts developing at the stage of beam existence and disappears in a certain time after beam interruption. The time of instability evolution is approximately 7 μsec, which agrees with experimental results.

The magnetic flux distribution shows that the internal magnetic flux is greater than the external one. As a result, during the evolution of tearing instability, the hot plasma from the center is ejected onto the chamber wall.

It is necessary to optimize the beam parameters so that the developing tearing instability remains internal, i.e., so that the energy is not ejected onto the chamber wall. For this purpose, the internal magnetic flux arising owing to the beam presence has to be smaller than the external magnetic flux.

This work was supported by the Russian Foundation for Basic Research (Grant No. 04-01-00244).

REFERENCES

1. A. V. Burdakov, A. V. Arzhannikov, V. T. Astrelin, et al., "Fast heating of ions in GOL-3 multiple mirror trap," in: *Proc. of the 31th Conf. on Controlled Fusion and Plasma Physics* (London, June 28–July 2, 2004) [CD-ROM], Vol. 27A, European Physical Society (2004), p. P4-156.
2. R. Yu. Akentjev, A. V. Arzhannikov, V. T. Astrelin, et al., "Multimirror open trap GOL-3: Recent results," *Trans. Fusion Technol.*, **43**, No. 1, 30–36 (2003).
3. B. B. Kadomtsev and O. P. Pogutse, "Nonlinear helical perturbations of the plasma in tokamaks," *Zh. Éxp. Teor. Fiz.*, **65**, No. 2, 575–589 (1973).
4. Yu. N. Dnestrovskii and D. P. Kostomarov, *Mathematical Modeling of the Plasma* [in Russian], Nauka, Moscow (1982).
5. D. Biskamp, "Nonlinear theory of the $m = 1$ mode in hot tokamak plasmas," *Phys. Rev. Lett.*, **46**, No. 23, 1522–1525 (1981).
6. E. Lazzaro, M. Ferrero, L. Gianoli, and L. Valdettaro, "Four-field description of fast reconnection of $m = 1$, $n = 1$ modes," *Phys. Scripta*, **61**, 624–627 (2000).
7. A. Y. Aydemir, "Nonlinear studies of $m = 1$ mode in high-temperature plasmas," *Phys. Fluids B*, **4**, No. 11, 3469–3472 (1992).
8. W. Xiagoang and A. Bhattacharjee, "Nonlinear dynamics of the $m = 1$ instability and fast sawtooth collapse in high-temperature plasmas," *Phys. Rev. Lett.*, **70**, No. 11, 1627–1630 (1993).
9. V. P. Zhukov, "Modeling of tearing instability in nonreduced two-fluid magnetohydrodynamics," *Fiz. Plazmy*, **31**, No. 8, 721–732 (2005).
10. G. I. Dudnikova, V. P. Zhukov, and G. Fuchs, "Density and total pressure behavior in the process of forces and spontaneous reconnection," *J. Appl. Mech. Tech. Phys.*, **40**, No. 4, 558–562 (1999).
11. L. A. Charlton, J. A. Holmes, V. E. Lynch, and B. A. Carreras, "Compressible linear and nonlinear resistive MHD calculations in toroidal geometry," *J. Comput. Phys.*, **86**, 270–293 (1990).
12. R. Lerbinger and J. F. Lucian, "A new semi-implicit method for MHD computations," *J. Comput. Phys.*, **97**, 444–459 (1991).
13. S. I. Braginskii, "Transport phenomena in plasma," in: *Problems in Plasma Theory* [in Russian], Vol. 1, Gosatomizdat, Moscow (1963), pp. 183–272.
14. L. D. Landau and L. M. Lifshits, *Electrodynamics of Continuous Media* [in Russian], Nauka, Moscow (1982).
15. K. Mohseni and T. Colonius, "Numerical treatment of polar coordinate singularities," *J. Comput. Phys.*, **157**, 787–795 (2000).
16. V. P. Zhukov, "Finite-difference scheme for solving two-fluid MHD equations in a cylindrical coordinate system," *Zh. Vychisl. Mat. Mat. Fiz.*, 45, No. 1, 156–169 (2005).
17. Yu. A. Berezin and M. P. Fedoruk, *Modeling of Unsteady Plasma Processes* [in Russian], Nauka, Novosibirsk (1993).